J Solid State Electrochem
DOI 10.1007/s10008-007-0339-8

ORIGINAL PAPER

Electron transfer at Au surfaces modified by Tethered Osmium bipyridine–pyridine complexes

Alejandra Ricci · Claudio Rolli · Silvina Rothacher · Luis Baraldo · Cecilia Bonazzola · Ernesto J. Calvo · Nicolas Tognalli · Alex Fainstein

Received: 15 January 2007 / Revised: 5 March 2007 / Accepted: 16 April 2007

Abstract Chemically modified electrodes by the osmium complex $\left[\mathrm{Os(bpy)_2Clpy}-X\right]^{+}\mathrm{PF_6^-}$ tethered to Au surfaces by (1) reaction of cysteamine with the aldehyde (X=CHO), (2) mercapto alkanoic acid reaction with amine [X=$(CH_2)_2NH_2$], and (3) reduction of the diazonium salt of p-aminobenzoic acid and further amidation reaction with the amine derivative of the osmium complex [X=$(CH_2)_2NH_2$] were performed to explore the electron transfer properties of these redox-modified surfaces. The modified Au surfaces were characterized by infrared reflection absorption spectroscopy and resonant Raman spectroscopy. Cyclic voltammetry was used to study the electrochemical properties of the osmium complexes covalently attached to the surface as a function of the type and length of the tether.

Keywords Diazonium · Thiol · SAM · Osmium bipyridil · Charge transfer · FTIR-RAS · Resonant Raman

Introduction

Design and control of modified electrode surfaces at the molecular level is of interest in electrocatalysis, biosensors, and molecular electronics. Nart et al. [1] reported a chemically modified Au electrode by $[Ru(CN)_5]^{3-}$ metal center as a π-donor system coordinated to the 4-mercaptopyridine ligand adsorbed on Au to design the first inorganic complex applicable to the assessment of the inherent rate of the cyt *c* electron transfer reaction.

A key point in that work was that the coordination of a π-donor transition metal center to a nitrogen on a pyridine ring of the 4-mercaptopyridine would affect its electronic density enhancing the C—S bond strength with consequent stability gain of the ad layer. The modified electrode was further characterized by infrared reflection spectroscopy to characterize the cyanide stretching frequency at 2,055 cm^{-1} that corresponds to the ligand of Ru(II) with no evidence of direct cyanide adsorbed at the Au electrode.

To modify electrode surfaces by grafting molecules in a well-controlled manner, Katz [2, 3] introduced the postfunctionalization of a functional thiol attached to Au electrodes. This strategy was used in our group by Molinero and Calvo [4] and Wheeldon et al. [5] to tether redox groups via thiolated surfaces.

While Au-thiol bond is the method of choice to tether redox groups at electrodes both in electrochemistry and molecular electronics, an alternative is the electro reduction of aryl diazonium salts to yield Au—C bond [6, 7]. The electrochemical reduction of diazonium salts has proven to be an excellent method to covalently attach molecules to carbon, silicon, AsGa, and metal surfaces [8, 9]. Besides C—C, C—Si, and C—Pt bonds, reactive metals such as Cu, Fe, Co, Ni, and Zn [10, 11] have been modified by aryl radicals produced from diazonium salts. In particular, C—Au bonds formed by electrochemical reduction of diazonium salts [6, 11, 12] and, more recently, Au nanoparticles [13] deserve special consideration because these molecular junctions can be compared to the very much studied thiol self-assembled

Dedicated to the memory of Professor Francisco (Chico) Nart.

A. Ricci · C. Rolli · S. Rothacher · L. Baraldo · C. Bonazzola · E. J. Calvo (✉)
INQUIMAE. Facultad de Ciencias Exactas y Naturales,
Universidad de Buenos Aires,
Pabellón 2, Ciudad Universitaria,
1428 Buenos Aires, Argentina
e-mail: calvo@qi.fcen.uba.ar

N. Tognalli · A. Fainstein
Centro Atómico Bariloche and Instituto Balseiro,
Comisión Nacional de Energía Atómica,
8400 San Carlos de Bariloche, Argentina

monolayers (SAMs). The difference in the energy of the valence atomic orbitals for C(2p) and Au(6s) is much lower that for S(3p) and Au(6f).

Modified surfaces by diazonium salt reduction have been characterized by X-ray photoelectron spectroscopy (XPS) [10–12, 14, 15], infrared [9–11, 13, 14, 16–18], and Raman spectroscopy [15, 18, 19]. However, spectroscopic evidence for monolayer formation on Au has been disclosed only very recently with s- and p-polarized Fourier transform infrared (FTIR) reflection-absorption spectroscopy (RAS). McCreery and coworkers have shown molecular orientation of nitro-azobenzene, azobenzene, nitro biphenyl, biphenyl, and fluorene tethered on graphitic carbon by attenuated total reflection FTIR and Raman spectroscopy [20]. The aryl diazonium salt of p-nitroaniline with further reduction of the nitro group to amine has been used to chemically bind DNA oligonucleotides to single-walled carbon nanotube electrodes [21].

The model osmium complex, $[Os(bpy)_2pyCl]^+$, and related compounds with replacement of the pyridine ligand with modified pyridines and tethered to surfaces have been reported by Abruña et al. [22–24], Forster et al. [24–29], Ulstrup et al., and others [30–32] bound by N—Au. In the present communication, we report the electrochemical behavior of the complex $[Os(bpy)_2PyCl]^+$ tethered to gold electrode surfaces previously modified with functionalized thiols or by diazonium salt reduction and further post functionalization with the osmium complex.

Experimental

Chemicals

The following chemicals were used as received: 4-aminomethylpyridine (Sigma-Aldrich, St. Louis, MO, USA), ethylene-glycol (Anedra, Buenos Aires, Argentina), ammonium hexafluorophosphate (Fluka, Buchs, Switzerland), 4-pyridincarboxy-aldehyde and p-toluensulfonic acid (Sigma-Aldrich), Toluene (Anedra), HCl (Mallinckrodt, Hazelwood, MO, USA), sodium hydrogen carbonate (Merck, Whitehouse Station, NJ, USA), 4-aminobenzoic acid (Sigma-Aldrich), fluoroboric acid 50% (Riedel-de-Haen, Morris, NJ, USA), *Iso*amyl nitrite (Sigma-Aldrich), diethyl ether (Cicarelli, Santa Fe, Argentina), tetrafluoroborate tetrabutylammonium (Fluka), acetonitrile (J. T. Baker, Phillipsburg, NJ, USA), cysteamine (Fluka), 3-mercaptopropionic acid, 11-mercaptoundecanoic acid (MUA) (Sigma-Aldrich), 16-mercaptohexadecanoic acid (MHDA) (Sigma-Aldrich), 1-ethyl-3-(3-dimethylaminopropyl)-carbodi-imide (Sigma-Aldrich), *N*-hydroxisuccinimide (Sigma-Aldrich), 4-2-hydroxyethyl-1-piperazineethanesulfonic acid (HEPES) sodium salt (Sigma-Aldrich), potassium nitrate (Merck), sodium cyanoborohydride (Sigma-Aldrich), ethanol (Sintorgan, Buenos Aires, Argentina), and methanol (Cicarelli).

Preparation of NH_2 derivatized osmium complex $[Os(bpy)_2Cl(py\text{-}CH_2\text{-}NH_2)]PF_6$

4-Aminomethylpyridine (19 mg, 0.178 mmol) and $[Os(bpy)_2Cl_2]^+$ (102 mg, 0.178 mmol) were dissolved in ethylene glycol (2 mL) in a Schlenk round-bottom flask. The solution was degassed twice with argon and heated with reflux for 3 h under argon atmosphere. After cooling, a NH_4PF_6 solution was added (1 mL) and the mixture was stirred for 30 min and filtered with a polyamide membrane (Ø 0.45 μm). The precipitate was washed with water and vacuum-dried [33, 34]. The preparation of CHO derivatized osmium complex $[Os(bpy)_2Cl(py\text{-}CHO)]PF_6$ has been reported elsewhere [35].

Protection of the aldehyde

4-Pyridinecarboxyaldehyde (1 g, 9.3 mmol), p-toluenesulfonic acid (200 mg, 0.2 mmol), and ethylenglycol (730 μL) were dissolved in toluene (100 mL) in a round bottom flask with a Dean–Stark trap. The mixture was heated with reflux for 4 h, and then, the toluene was vacuum-evaporated.

Synthesis of the osmium complex

4-Pyridinecarboxy acetal (0.795 g, 5.3 mmol) and $[Os(bpy)_2Cl_2]^+$ (0.164 g, 0.3 mmol) were dissolved in 25 mL water/ethanol (1:1) solution, the system was degassed twice with argon and refluxed for 9 h.

Unprotection of the aldehyde

The obtained complex was dissolved in 1 M HCl (3 mL of 1 M HCl every 18 mg of complex) and this solution was degassed with argon and heated to 60 °C for 2 h. Finally, it was neutralized with $NaHCO_3$ until pH=7 and freeze dried.

Preparation of 4-carboxy-phenyl diazonium salt tetrafluoroborate

4-Aminobenzoic acid (0.4 g, 2.91 mmol) was dissolved in ethanol (1 mL) and aqueous tetrafluoroboric acid solution (50% solution: 0.65 mL, 3.7 mmol); the mixture was then cooled to 0 °C. *Iso*amyl nitrite (0.6 ml, 4.5 mmol) was added dropwise to the mixture and stirring continued for 30 min. Dilution of the mixture with diethyl ether (30 mL) led to the precipitation of 4-benzoic acid diazonium tetrafluoroborate as light yellow crystals. The IR spectra resulted in ν_{max}(KBr)/cm^{-1} 3,494, 3,424, 3,093, 3,072,

2,933, 2,651, 2,551, 2,293, 1,725, 1,409, 1,373, 1,311, 1,203, 1,066, and 806 [36].

Modification of Au electrodes by grafting benzoic acid through diazonium salt reduction

Silicon (100) substrates were coated with a 20-nm titanium and 20-nm palladium adhesion layer and a 200-nm gold layer, thermally evaporated with an Edwards Auto 306 vacuum coating system at $P<1.10^{-8}$ bar, and employed as electrodes.

A glass electrochemical cell with a Pt counter electrode and a Ag/AgCl, 3 M KCl reference electrode was employed, and potentials herein are reported with respect to this reference.

Benzoic acid was tethered to gold surfaces by electrochemical reduction of the corresponding diazonium salt using chronoamperometry (0.4 V, 5 min in 5 mM 4-carboxy-phenyl diazonium salt tetrafluoroborate/0.1 M tetrabutylammonium tetra-fluoro borate/acetonitrile).

Modification of Au electrodes by grafting thiols

The gold electrodes were dipped in 1 mM 3-mercaptopropionic, 11-mercaptoun-decanoic acid, and 16-mercaptohexadecanoic acid in ethanol, and in 0.13 mM cysteamine/water solution, respectively, for 2 h.

Bonding of osmium complexes to the modified gold surfaces

The surfaces modified with benzoic, 3-mercaptopropionic, 11-mercaptoundecanoic, and 16-mercaptohexadecanoic acids were incubated in 40 mM 1-ethyl-3-(3-dimethyl-aminopropyl)-carbodiimide/10 mM *N*-hydroxy succinimide solution for 1 h, and then, they were dipped in 0.25 mM $\left[Os(bpy)_2CI(py-CH_2-NH_2)\right]^+PF_6^- \Big/$ 0.05M HEPES buffer (*N*-2-hydroxyethylpiperazine-*N*′-2-ethanesulfonic acid) pH=7.3, I=0.1 M KNO_3 for 24 h. This way, an amide bond was formed between the amino group in the complex and the acid group on the surface. The surface modified with cysteamine was immersed overnight in 0.075 mM $[Os(bpy)_2Cl(py\text{-}CHO)]^+$/2 mM $NaBH_3CN$/methanol solution of pH 5.

All osmium complexes were studied by NMR spectroscopy to assess for possible contamination of free ligand, which, if present, would postfunctionalize the thiolated Au surface.

FTIR experiment

After surface modification, FTIR-RAS spectra were collected, using a Nicolet 560 FTIR spectrometer equipped with cryogenic MCT-A detector, a zinc selenide (Nicolet, Spectratech, Hong Kong, China) polarizer, and a Whatman 75-52 purge gas generator. A bare Au surface was employed as reference, and the spectra for p- and s-polarized radiation were collected with a spectral resolution of 4 cm^{-1} accumulating 200 scans. No data smoothing was employed. Experimental details have been published elsewhere [7].

Raman experiment

The resonant Raman scattering experiments were performed using a Jobin–Yvon T64000 triple spectrometer operating in subtractive mode and equipped with a liquid N_2 cooled charge coupled device. The excitation was done using energies between 1.916 eV (647 nm) and 2.707 eV (458 nm) from the 11 lines of an Ar—Kr ion laser. The power used was 30 mW, concentrated on a line focus, ≈2 mm long and ≈100 μm wide. A line focus was chosen to reduce the photon-induced degradation of the osmium complex (photobleaching by ligand exchange aquation of the pyridine ligands). The resonant Raman experiments were performed in air.

Electrochemical experiment

Electrochemical measurements were carried out with an Autolab V30 system (Eco Chemie, Utrecht, the Netherlands) controlled by a General Purpose Electrochemical Software (GPES) with 750-kHz bandwidth ADC750 fast sampling module and scangen analog sweep module. All experiments were carried out at room temperature (20±2°C) in a purpose-built, three-electrode Teflon cell, with an electrode exposed area of approximately 0.25 cm^2 delimited by an inert "o" ring. As reference electrode, Ag/AgCl, 3 M KCl was employed, and all electrode potentials herein are referred to it; a platinum gauze auxiliary electrode of large area was employed. Before thiol adsorption, the electrode potential was cycled in 2 M sulfuric acid between 0.2 and 1.6 V at 0.1 V s^{-1} to check for surface contamination, and electrochemically active areas were calculated from the reduction peak of gold oxide. The uncompensated solution resistance was measured by a current interruption technique implemented in the GPES.

Results and discussion

The different strategies to tether the osmium complex $[Os(bpy)_2Clpy\text{-}X]^+PF_6^-$ to Au surfaces are depicted in Schemes 1, 2, and 3 for (1) cysteamine reaction with the aldehyde derivative and further reduction of the Schiff base formed, (2) mercapto alkanoic acid reaction with the amine derivative to yield an amide link, and (3) reduction of the diazonium salt of p-amino benzoic acid and further

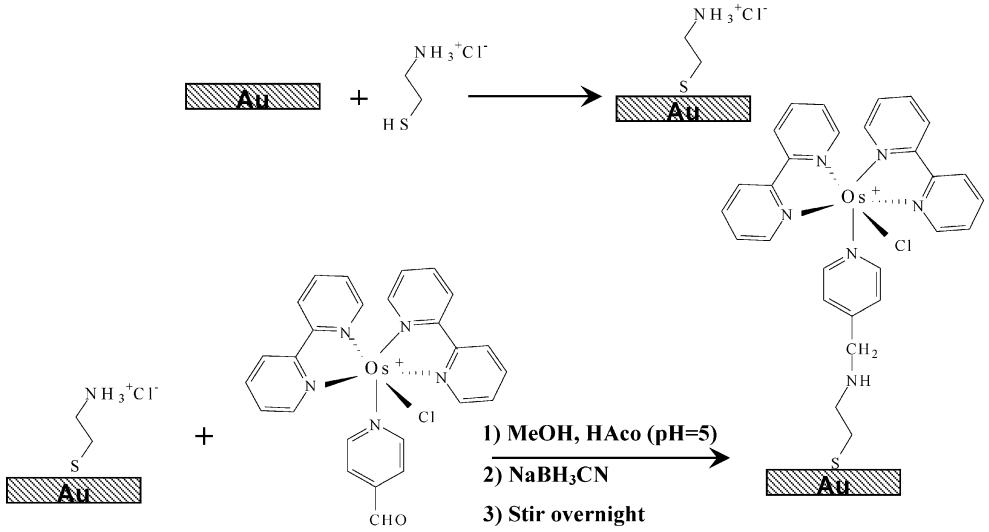

Scheme 1 Schematic of $[Os(bpy)_2Cl(py\text{-}CH_2\text{-}CHO)]^+$ immobilized covalently on monolayers of cysteamine on gold surfaces

amidation reaction with the amine derivative of the osmium complex.

Infrared characterization

We shall first examine the chemically modified gold surfaces with spectroscopic techniques to prove that the cartoons in Schemes 1, 2, and 3 describe the chemistry on those surfaces, i.e., the existence and geometry of the different functional groups tethered to the surface. Then, we shall proceed with the electrochemical analysis.

FTIR-RAS of Au surfaces modified by alkanoic (MUA and MHDA) and mercaptobenzoic acid (MBA) provide information about the presence of IR-active functional groups at the surface and also about the orientation of the transition dipole moments with respect to the surface [37].

The FTIR-RAS spectra of Au surfaces modified by MUA and MBA are shown in Fig. 1a and b, respectively. The main IR features in Fig. 1a are consistent with the reported spectra of MUA [38–40] and MHDA [37] SAMs on Au, i.e., asymmetric ν_{aCOOH} at 1,730 cm^{-1} due to free carboxylic acid, H-bonded symmetric ν_{sCOOH} at 1,707 cm^{-1}, and methylene $\nu_{SC\text{-}H}$ at 2,848 and $\nu_{aC\text{-}H}$ at 2,918 cm^{-1}.

The FTIR-RAS spectra of 4-, 3-, and 2-MBA have been reported by Crooks et al. [41]. The spectrum depicted in Fig. 1b for MBA shows the stretching bands at 1,730 and 1,707 cm^{-1}, which are assigned to two distinct types of COOH: weakly H-bonded or free COOH at 1,730 cm^{-1} and H-bonded at 1,707 cm^{-1} [37], while the bands observed at 1,540 and 1,419 cm^{-1} can be associated with the asymmetric C—O stretching and symmetric stretching vibration of COO^-, respectively [39]. Band at 1,608 cm^{-1} can be assigned to the benzene ring mode $\nu_{C\text{-}C}$, and the peak at 1,419 cm^{-1} could be due to either $\nu_{C\text{-}C}$ or to ν_{sCOO}^{-} [41]. The CN_2^+ vibrations at 2,280–2,300 cm^{-1} found in the diazonium salts (KBr pellet, not shown) are absent in the

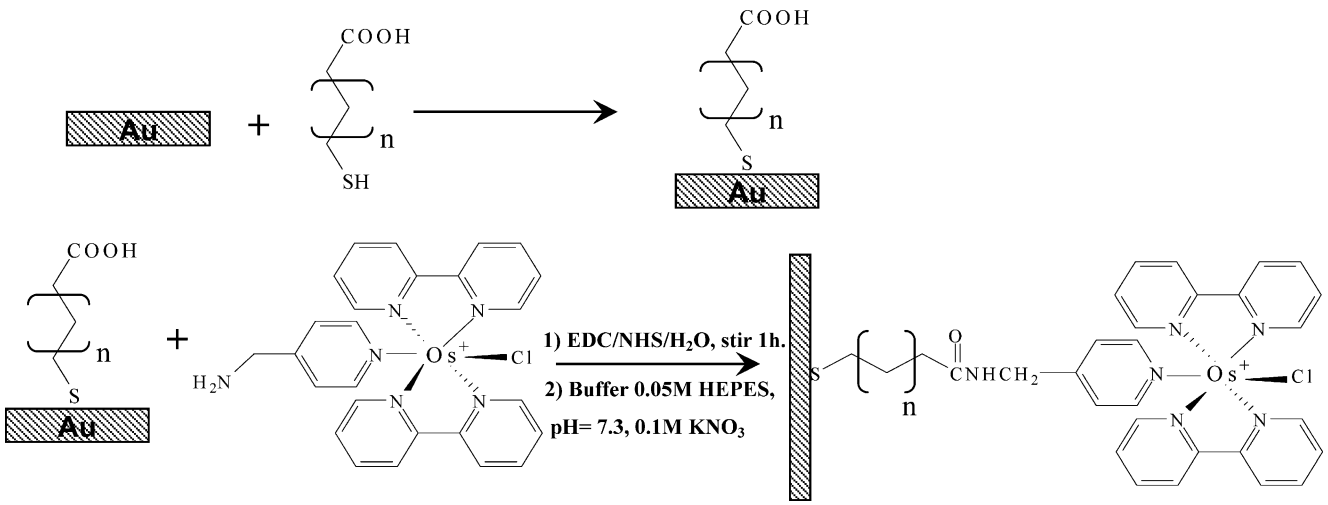

Scheme 2 Schematic of $[Os(bpy)_2Cl(py\text{-}CH_2\text{-}NH_2)]^+$ immobilized covalently on monolayers of mercaptoalkanoic acids on gold surfaces

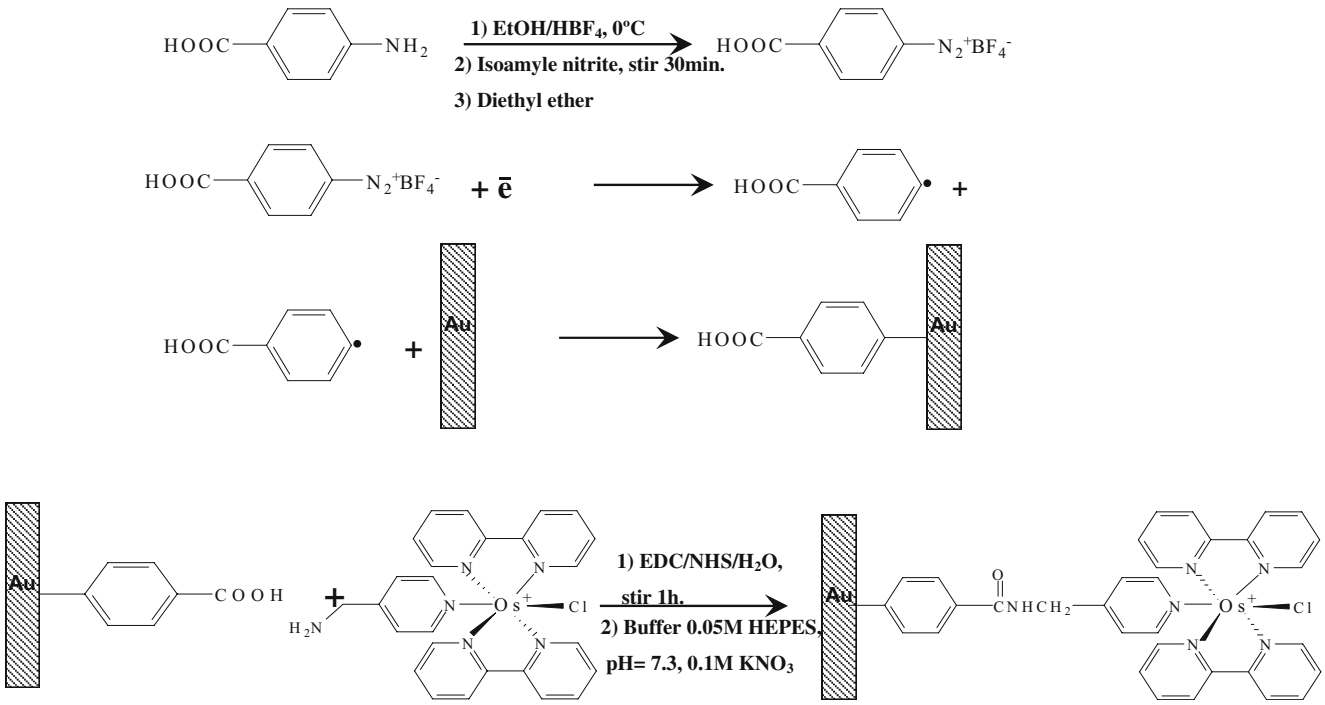

Scheme 3 Schematic of $[Os(bpy)_2Cl(py\text{-}CH_2\text{-}NH_2)]^+$ on monolayers of aryl linked benzoic acid on gold surfaces

reflectance spectra of Fig. 1b confirming the loss of N_2 upon electroreduction and formation of the aryl radical on the Au surface, as has been shown for the p-nitrophenyl derivative [7].

Surface selection rules for IR reflection at metals determine that the molecule attached to the surface with a component of a dynamic transition moment perpendicular to that surface are observed when p-polarized light is used [42] because the vibrational modes whose transition dipole moments are perpendicular to the surface show maximal absorbances, while the vibrational modes whose transition dipole moments are parallel to the surface show no absorbance. Thus, the planar COOH group active in the infrared for p-polarized radiation should have a perpendicular orientation with respect to the Au surface.

Raman spectroscopic characterization of the osmium complex

Resonant Raman scattering of the complex $[Os(bpy)_2 Clpy-X]^+PF_6^-$ tethered to the surface was observed by exciting with 11 laser lines from 647 to 457 nm, with maximum Raman intensity at 514.5 nm, as previously reported for similar Os-complexes [43]. This energy corresponds to the laser excitation resonant with the charge transfer transition from the osmium to the ligands (pyridine and 2,2′-

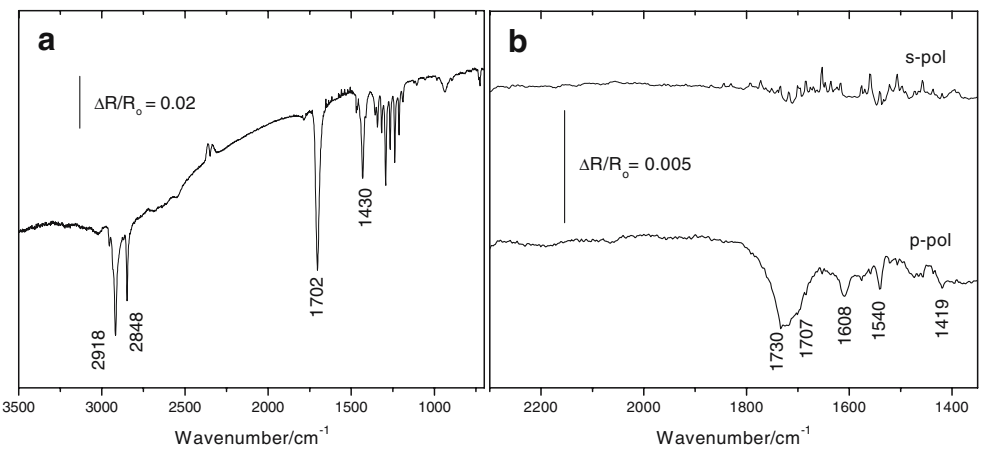

Fig. 1 FT-IRRAS spectra of a gold surface modified with 11-mercaptoundecanoic acid (**a**) and aryl diazonium linked benzoic acid (**b**). Resolution of 4 cm^{-1}, accumulation of 200 scans

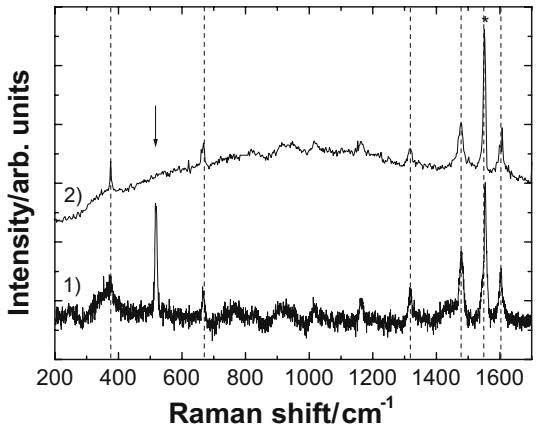

Fig. 2 Resonat Raman spectra for $[Os(bpy)_2Cl(py\text{-}CHO)]^+$ and $[Os(bpy)_2Cl(py\text{-}CH_2\text{-}NH_2)]^+$ tethered to the surface by cysteamine (1) and aryl diazonium linked salt (2), respectively. Spectra were collected under typical conditions using 30 mW and 600 s of the λ=514.5 nm line of an Ar—Kr laser

bipyridines) [49]. Figure 2 presents the resonant Raman spectra for $[Os(bpy)_2Cl(py\text{-}CHO)]^+$ and $[Os(bpy)_2Cl(py\text{-}CH_2\text{-}NH_2)]^+$ tethered to the surface by cysteamine (1) and aryl diazonium linked salt (2), respectively. All major peaks in Fig. 2 (dashed lines) can be assigned to the complex $[Os(bpy)_2Cl\text{-}X]^+$, namely, 380 cm^{-1} associated with a vibration of the Os—N bond, 668 cm^{-1} related to a pyridine bending mode, and the four peaks at 1,321, 1,480, 1,550, and 1,612 cm^{-1} related to pyridine stretching vibrations. The Raman signal centered at 516.5 cm^{-1} (arrow) in the spectrum of the Os complex attached by the cysteamine is probably related to the S—C stretching between the S atom attached to the Au substrate and its C neighbor [44] and it is consistently absent in the other spectra (2). We mention that the narrow peak at 1,555 cm^{-1} (labeled with an asterisk) comes from the substrate, and we used it to normalize the spectral intensities. It can be concluded from these data that the osmium 2,2′-bipyridyl-pyridine complex is present and its

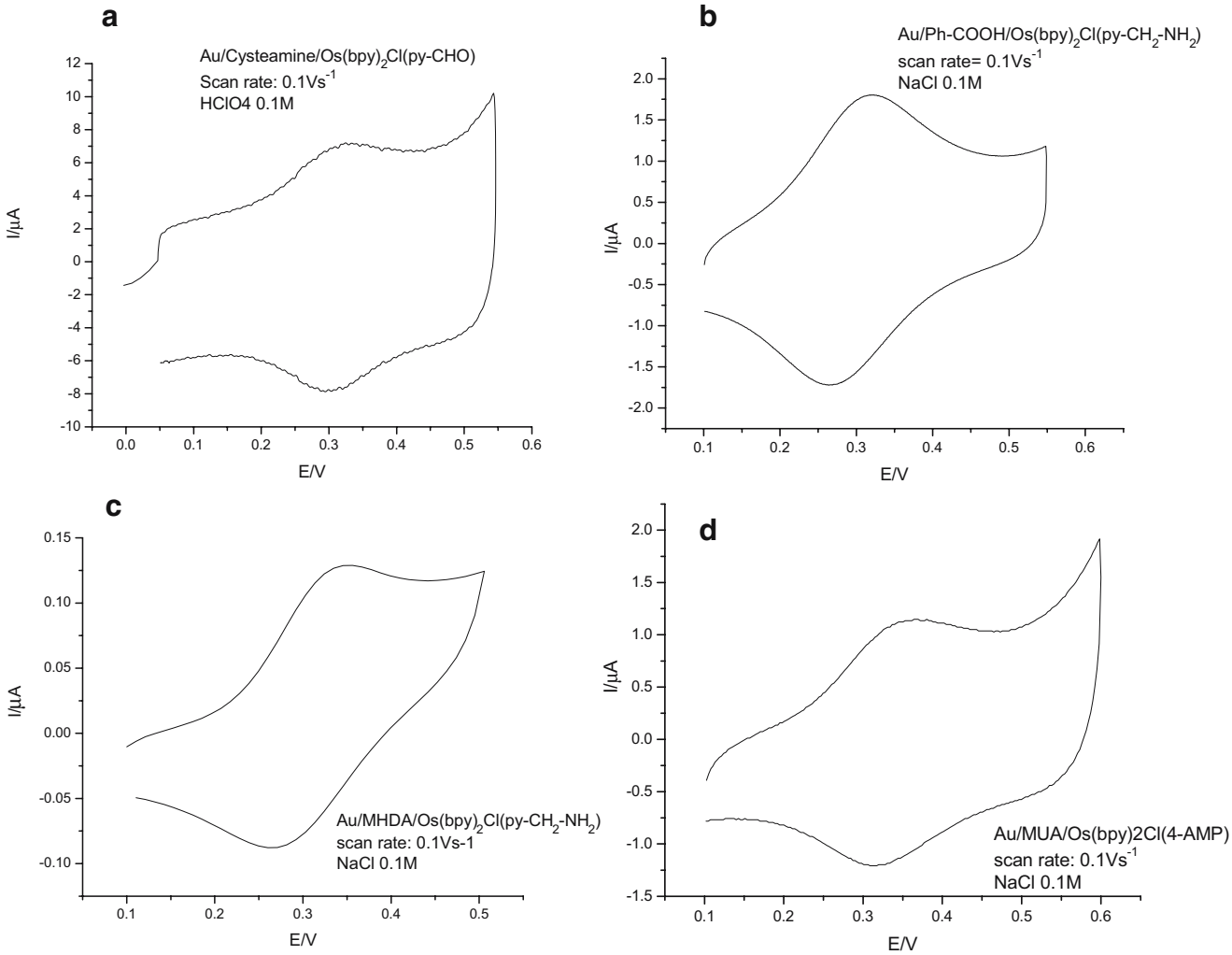

Fig. 3 Cyclic voltammetry of **a** Au/Cysteamine/$[Os(bpy)_2P_yCl]^+$ in 0.1 M $HClO_4$, **b** Au/Ph-COOH/$[Os(bpy)_2Cl(py\text{-}CH_2\text{-}NH_2)]^+$, **c** Au/MHDA/$[Os(bpy)_2Cl(py\text{-}CH_2\text{-}NH_2)]^+$ 0.1 M, and **d** Au/MUA/$[Os(bpy)_2Cl(py\text{-}CH_2\text{-}NH_2)]^+$ in 0.1 M NaCl at 0.1 V s^{-1}

Table 1 Electrochemical parameters for different modifications of Au with $[Os(bpy)_2PyCl]^+$

	AuSC2-Os	AuSC3-Os	AuSC11-Os	AuSC16-Os	AuPh-Os
E_{app}/V	0.300	0.325	0.350	0.318	0.295
ΔE_p/V	0.035	0.040	0.015	0.040	0.050
Q_{redox}/μC cm^{-2}	2.12	1.81	3.13	2.36	1.74
FWHH	0.123	0.112	0.123	0.110	0.147
k/s^{-1}	–	250	1,870	8	98

structure remains intact in both samples. The ability to link the complex to the Au surface seems to be similar for the two building strategies, as can be deduced from the comparable intensities.

Further confirmation of the presence of osmium on the surface was obtained by XPS 4f signal (50.7 eV) partly overlapped to the Au 5p signal (56.8 eV). The estimated osmium surface coverage by XPS coincides with the electrochemically determined value (see below).

Electrochemical results

The electrochemistry of monolayer of $[Os(bpy)_2Clpy\text{-}X]PF_6$ tethered on Au electrode surfaces by different methods has been investigated by cyclic voltammetry in the scan rate range from 10 mV s^{-1} to 100 V s^{-1}. Typical cyclic voltammograms at 0.1 V s^{-1} are depicted in Fig. 3 for (a) AuS-C2 (cysteamine) in 0.1 M $HClO_4$, (b) Au—Ph (benzoic acid), (c) AuS-C16 (MHDA), and (d) AuS-C11 (MUA) in 0.1 M NaCl. In all cases, a linear relationship between the peak current and scan rate, and the ratio of cathodic to anodic charge close to one at low scan rate, indicate that the osmium complex is attached to the Au surface and that it can be oxidized and reduced completely.

The electrochemical properties of these osmium bipyridine–pyridine monolayers are summarized in Table 1, where a comparison of the redox potential, peak potential separation, charge density, and full width at half maximum (FWHM) is presented.

The redox potential of the complex chemically attached to the surface ranges from 0.295 to 0.350 V, as compared to the value 0.260 V for this complex in solution. These values are in good agreement with previous reports for this and similar complexes adsorbed on electrode surfaces. The discrepancy with the value in solution and the variation in the different modified electrodes is due to the electrostatic work terms because the concentration of the anion balancing charge determines the interfacial potential [50]. Donnan potential determined by the relative activities of counter ions in the solution and on the surface [45] is:

$$Os(bpy)_2pyCl^{2+}_{surf} + nCl^-_{surf} + e(Au) \rightarrow Os(bpy)_2pyCl^+_{surf} + (n-1)Cl^-_{surf} + Cl^-_{soln} \quad (1)$$

The apparent potential of the working electrode is, thus, E_{app}:

$$E_{app} = E^O + \frac{RT}{F}\ln\frac{a(Os(III))a(Cl^-_{surf})}{a(Os(II))a(Cl-sol)} \quad (2)$$

where the redox potential of the osmium monolayer depends on the activities of Os(III) and Os(II) and chloride

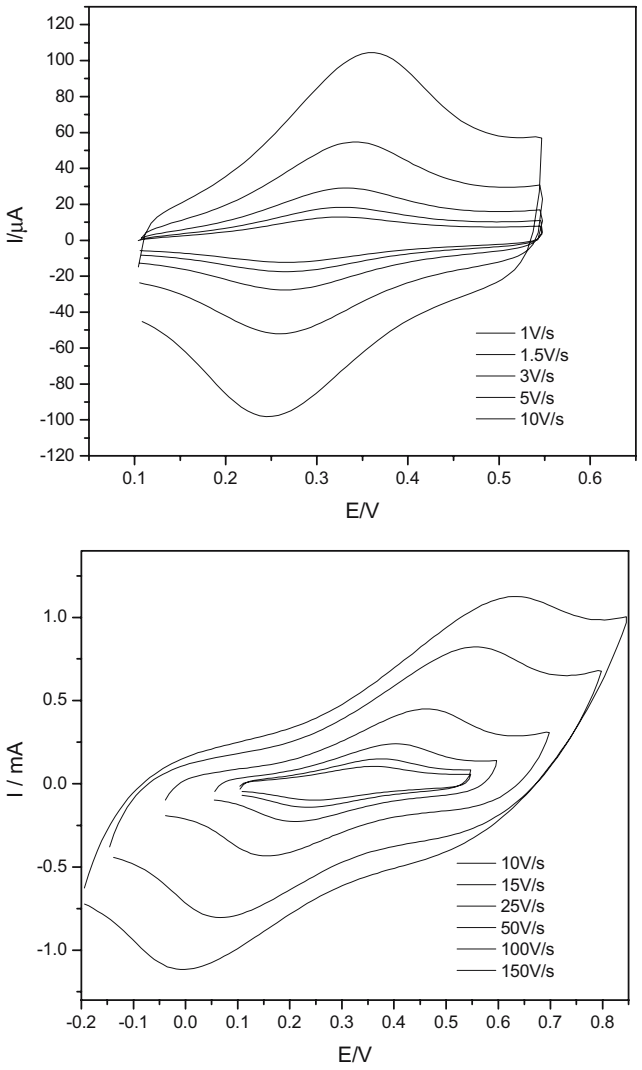

Fig. 4 Cyclic voltammetry of Au/Ph-COOH/$[Os(bpy)2Cl(py\text{-}CH\text{-}NH_2)]^+$ in 0.1 M NaCl at different scan rates from 1 to 150 V s^{-1}

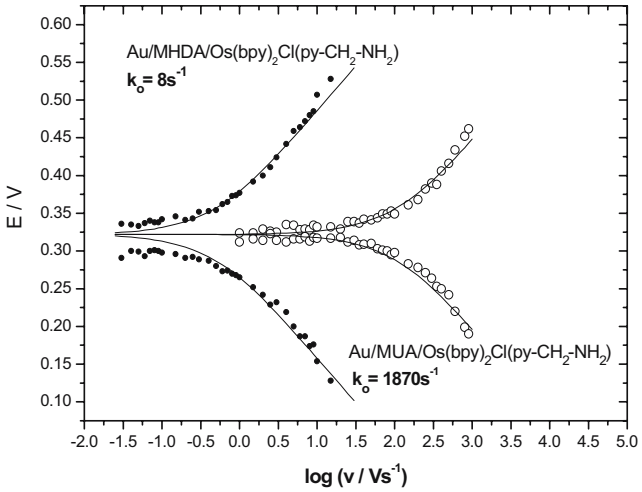

Fig. 5 Plot of Ep vs log (sweep rate) for a gold surface modified with MUA/$[Os(bpy)_2Cl$ (py-CH_2-$NH_2)]^+$ and MHDA/$[Os(bpy)_2Cl$(py-CH_2-$NH_2)]^+$, respectively. The experimental data are denoted by *closed* and *open circles*. The *solid lines* are best fit to Laviron model for α=0.5 with k_o=8 and 1,870 s^{-1}, respectively. The supporting electrolyte is 0.1 M NaCl

at the surface and the activity of chloride in the electrolyte. The activity of chloride on the surface will be determined by the net positive charges at the electrode surface with the contribution of the osmium complex and the effect of dissociated carboxylates. Thus, the equilibrium constant given by the logarithmic term in Eq. 2 will be different in each osmium monolayer.

The surface redox cyclic voltammograms are nonideal with a peak separation $\Delta E_p>0$, even for very low scan rates and a full potential width at half maximum, FWHM larger than the value expected for an ideal one-electron redox process, ca. 90.6 mV, which is consistent with a weak repulsive interaction between the surface sites [46, 47].

Integration of the redox charge under the anodic and cathodic peaks yields values that are consistent with previous reports of similar osmium complexes adsorbed on surfaces via pyridines [22–26]. The surface coverage by osmium redox species in all cases is lower than the maximum coverage of 90 pmol cm^{-2} (8.6 μC cm^{-2}) for a closed packed structure on the basis of molecular size, 185 $Å^2$.

While previous reports described osmium pyridine–bipyridine complexes adsorbed on metal electrodes via the nitrogen atom of the pyridines [24], in this work, we have introduced postfunctionalization of carboxylated alkane thiols of different lengths, C2, C3, C11, and C16, and grafted benzoic acid via electroreduction of the corresponding diazonium salt. In the latter case, Fig. 4 shows a comparison of selected cyclic voltammograms of Au/Ph-CONH$[Os(bpy)_2ClPy]^+$ in 0.1 M NaCl as the scan rate, v, is systematically varied in a wide range from 10 mVs^{-1} to 150 Vs^{-1}. Gooding and coworkers reported the postfunctionalization with ferrocenemethylamine of mercapto benzoic acid and 4-carboxyphenyl monolayers grafted by reduction of diazonium salts on glassy carbon and gold electrode surfaces [6].

The exponential dependence of the rate of electron transfer with the distance between the osmium center and the electrode surface is expected for direct electron tunneling [48]. By using long tethers, the tunneling barrier decreases the fast electron transfer rate of the osmium complex to sufficiently slow values that can be measured at high overpotentials as shown in the Trumpet plots depicted in Fig. 5 [54].

The kinetics of the heterogeneous electron transfer to and from the osmium complexes tethered to Au surfaces has been determined from the variation of the corresponding anodic and cathodic peak positions as a function of the scan rate. Trumpet plots, E_p vs log v, are shown in Fig. 5 for C11 and C16, and the line is the best fit to the Laviron treatment [46, 47] for α=0.5 and k_s=1,870 and 8 s^{-1}, respectively, which is consistent with an exponential decay with the length of

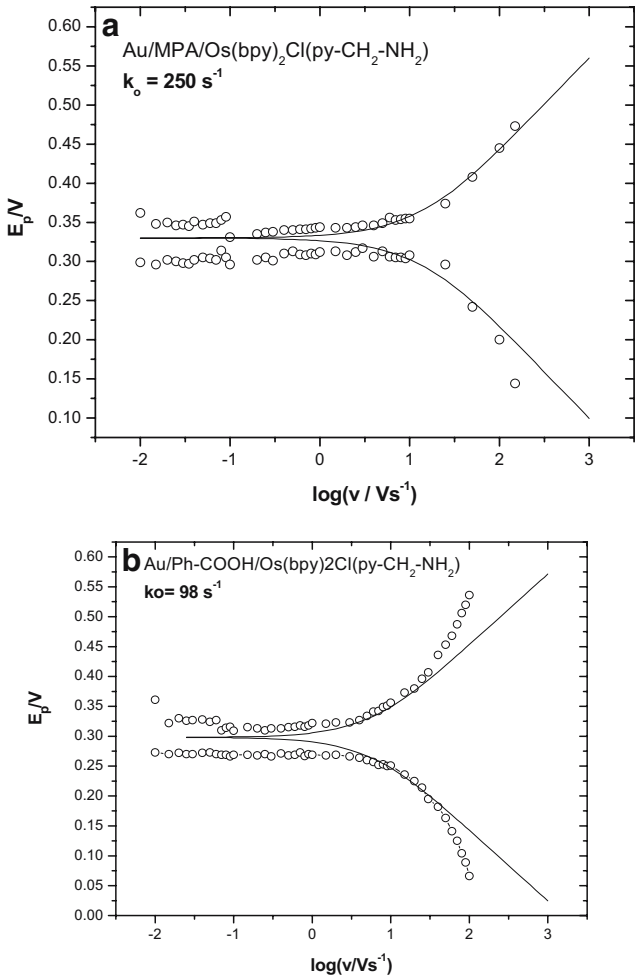

Fig. 6 Plot of Ep vs log (sweep rate) for a gold surface modified with **a** mercapto propanoic acid/$[Os(bpy)_2$ Cl(py-CH_2-$NH_2)]^+$ and **b** PhCOOH/$[Os(bpy)_2Cl$(py-CH_2-$NH_2)]^+$. The experimental data are denoted by *circles*. The *solid lines* are the best fit to Laviron for α= 0.5 model with k_o=250 and 98 s^{-1}, respectively. The supporting electrolyte is 0.1 M NaCl

the tether as previously reported for ferrocene [48] and ruthenium pentamine [49, 50] moieties chemically bound to the gold surface by alkane carboxyamides.

Laviron treatment is based on the Butler–Volmer approximation, which is valid for overpotentials much smaller than the reorganization energy of the redox reaction, $\eta << \lambda$, and assumes a constant transfer coefficient, α, which should result in linear Trumpet plots at high sweep rates [51–53]. Figure 6 depicts Trumpet plots for mercapto propanoic acid and benzoic acid (Au—Ph), respectively, chemically bound to the amine derivative of the osmium bipyriridine–pyridine in 0.1 M NaCl. At sweep rates larger than 10 V s^{-1}, nonlinear dependence of peak potential on sweep rate results in heterogeneous rate constants derived from the Laviron mechanism. However, by fitting the experimental data over a limited range of sweep rates, the values of k_s=250 and 98 s^{-1}, respectively, were obtained, which are consistent with similar values for ferrocene chemically attached via aryl diazonium bond to glassy carbon and gold [6]. The kinetic data are compiled in Table 1.

Potential dependent transfer coefficients, α, are consistent with the nonlinearity observed in the Trumpet plots, which can be explained by the Marcus theory of electron transfer at high overpotential. We rule out ohmic drop [54] as the main cause of the nonlinear behavior because the uncompensated solution resistance in these experiments is less than 10 Ω, and the largest current densities in the cyclic voltammetry would yield ohmic drops less than 10 mV, while the deviations from Laviron linear plots are much larger.

Conclusions

We have modified Au surfaces with $[Os(bpy)_2Clpy]PF_6$ by different strategies using postfunctionalization of carboxyaldehyde and carboxylic acid alkane thiols of different lengths, C2, C3, C11, and C16, and grafted benzoic acid via electroreduction of the corresponding diazonium salt. The orientation of the molecules has been assessed by FTIR-RAS spectroscopy and the integrity of the $[Os(bpy)_2Clpy]^+$complex has been demonstrated by resonance Raman spectroscopy.

The electrochemical behavior of the osmium complex tethered by different strategies to the Au electrodes has been investigated by cyclic voltammetry as a function of the tether length and the nature of the surface link (i.e., Au—S or Au—C). Very fast electron transfer rates have been observed for the Os(III)/Os(II) surface redox couple with the exponential decay with tether distance expected for direct electron tunneling.

Acknowledgement The authors wish to dedicate this scientific contribution to the memory of Professor Francisco (Chico) Nart. The authors are grateful to Consejo Nacional de Investigaciones Científicas y Técnicas, University of Buenos Aires, and Agencia Nacional de Promoción Científica y Tecnológica (PICT 06-17170) for financial support. The authors wish to thank Dr. Federico Williams for the XPS measurements and helpful discussions.

References

1. Diogenes ICN, Nart FC, Moreira IS (1999) Inorg Chem 38:1646
2. Katz EY (1990) J Electroanal Chem 291:257
3. Katz EY, Solovev AA (1990) J Electroanal Chem 291:171
4. Molinero V, Calvo EJ (1998) J Electroanal Chem 445:17
5. Calvo EJ, Rothacher MS, Bonazzola C, Wheeldon IR, Salvarezza RC, Vela ME, Benitez G (2005) Langmuir 21:7907
6. Liu GZ, Liu JQ, Bocking T, Eggers PK, Gooding JJ (2005) Chem Phys 319:136
7. Ricci A, Bonazzola C, Calvo EJ (2006) Phys Chem Chem Phys 8:4297
8. Bahr JL, Tour JM (2001) Chem Mater 13:3823
9. Delamar M, Desarmot G, Fagebaume O, Hitmi R, Pinson J, Saveant JM (1997) Carbon 35:801
10. Adenier A, Cabet-Eliry E, Chaussé A, Griveau S, Mercier F, Pinson J, Vautrin-Ul C (2005) Chem Mater 17:491
11. Bernard MC, Chausse A, Cabet-Deliry E, Chehimi MM, Pinson J, Podvorica F, Vautrin-Ul C (2003) Chem Mater 15:3450
12. Laforgue A, Addou T, Belanger D (2005) Langmuir 21:6855
13. Mirkhalaf F, Paprotny J, Schiffrin DJ (2006) J Am Chem Soc 128:7400
14. Allongue P, Delamar M, Desbat B, Fagebaume O, Hitmi R, Pinson J, Saveant JM (1997) J Am Chem Soc 119:201
15. Liu Yc, McCreery RL (1995) J Am Chem Soc 117:11254
16. Pinson J, Podvorica F (2005) Chem Soc Rev 34:429
17. Kariuki JK, McDermott MT (2001) Langmuir 17:5947
18. McCreery RL, Viswanathan U, Kalakodimi RP, Nowak AM (2006) Faraday Discuss 131:33
19. Nowak AM, McCreery RL (2004) Anal Chem 76:1089
20. Anariba F, Viswanathan U, Bocian DF, McCreery RL (2006) Anal Chem 78:3104
21. Lee CS, Baker SE, Marcus MS, Yang WS, Eriksson MA, Hamers RJ (2004) Nano Lett 4:1713
22. Acevedo D, Abruna HD (1991) J Phys Chem 95:9590
23. Acevedo D, Bretz RL, Tirado JD, Abruna HD (1994) Langmuir 10:1300
24. Forster RJ, Figgemeier E, Loughman P, Lees A, Hjelm J, Vos JG (2000) Langmuir 16:7871
25. Forster RJ (1996) Inorg Chem 35:3394
26. Forster RJ, Faulkner LR (1994) J Am Chem Soc 116:5444
27. Forster RJ, Keyes TE, Majda R (2000) J Phys Chem B 104:4425
28. Forster RJ, Loughman P, Keyes TE (2000) J Am Chem Soc 122:11948
29. Forster RJ, O'Kelly JP (2001) J Electrochem Soc 148:E31
30. Albrecht T, Guckian A, Ulstrup J, Vos JG (2005) Nano Lett 5:1451
31. Albrecht T, Guckian A, Ulstrup J, Vos JG (2005) IEEE Trans Nanotechnol 4:430
32. Albrecht T, Moth-Poulsen K, Christensen JB, Guckian A, Bjornholm T, Vos JG, Ulstrup J (2006) Faraday Discuss 131:265
33. Haddox RM, Finklea HO (2004) J Phys Chem B 108:1694
34. Kober EM, Caspar JV, Sullivan BP, Meyer TJ (1988) Inorg Chem 27:4587
35. Danilowicz C, Corton E, Battaglini F (1998) J Electroanal Chem 445:89
36. Kizil M, Yilmaz EI, Pirinccioglu N, Aytekin C (2003) Turk J Chem 27:539
37. Yan L, Marzolin C, Terfort A, Whitesides GM (1997) Langmuir 13:6704

38. Futamata M (2003) J Electroanal Chem 550:93
39. Johann R, Vollhardt D, Mohwald H (2001) Colloids Surf A Physicochem Eng Asp 182:311
40. Jordan CE, Frey BL, Kornguth S, Corn RM (1994) Langmuir 10:3642
41. Wells M, Dermody DL, Yang HC, Kim T, Crooks RM, Ricco AJ (1996) Langmuir 12:1989
42. Urban MW (1993) Vibrational spectroscopy of molecules and macromolecules on surfaces. Wiley, New York
43. Tognalli N, Fainstein A, Bonazzola C, Calvo E (2004) J Chem Phys 120:1905
44. Abdelsalam ME, Bartlett PN, Baumberg JJ, Cintra S, Kelf TA, Russell AE (2005) Electrochem Commun 7:740
45. Redepenning J, Tunison HM, Finklea HO (1993) Langmuir 9:1404
46. Laviron E (1979) J Electroanal Chem 101:19
47. Laviron E, Roullier L (1980) J Electroanal Chem 115:65
48. Chidsey CED (1991) Science 251:919
49. Finklea HO, Hanshew DD (1992) J Am Chem Soc 114:3173
50. Ravenscroft MS, Finklea HO (1994) J Phys Chem 98:3843
51. Tender L, Carter MT, Murray RW (1994) Anal Chem 66:3173
52. Napper AM, Liu HY, Waldeck DH (2001) J Phys Chem B 105:7699
53. Weber K, Creager SE (1994) Anal Chem 66:3164
54. Roullier L, Laviron E (1983) J Electroanal Chem 157:193